ELSEVIER

Contents lists available at ScienceDirect

Mathematical Biosciences

journal homepage: www.elsevier.com/locate/mbs



Original Research Article

Physics-based modeling of Age-related Macular Degeneration—A theoretical approach to quantify retinal and choroidal contributions to macular oxygenation



Alice C. Verticchio Vercellin ^a, Alon Harris ^{a,*,1}, Greta Chiaravalli ^{b,c}, Riccardo Sacco ^d, Brent Siesky ^a, Thomas Ciulla ^e, Giovanna Guidoboni ^f

- a Department of Ophthalmology, Icahn School of Medicine at Mount Sinai, New York, NY, United States of America
- b Italian Institute of Technology, Milano, Italy
- ^c Dipartimento di Fisica, Politecnico di Milano, Italy
- d Dipartimento di Matematica, Politecnico di Milano, Italy
- e Vitreoretinal Medicine and Surgery, Midwest Eye Institute, Indianapolis, IN 46290, United States of America
- Department of Electrical Engineering and Computer Science, Department of Mathematics, University of Missouri, Columbia, MO, United States of America

ARTICLE INFO

MSC:

99-00

Keywords: Macula Retina

ABSTRACT

We developed a mathematical model to characterize how macular oxygenation may be affected by abnormalities in the retinal and choroidal oxygen supplies. The macular region is modeled as a layered structure including: ganglion cell and nerve fiber layers, inner plexiform layer, inner nuclear layer, outer plexiform layer, outer nuclear layer, inner segment of photoreceptors layer and retinal pigmented epithelium. Each layer is characterized by specific levels of oxygen consumption. The vitreous and the choroid are located at the macula boundary and provide oxygen via boundary conditions of Dirichlet type. The three capillary plexi (superficial, intermediate, and deep) of the retinal circulation pierce the macular layers and provide oxygen via a volumetric source that depends on the retinal blood flow. Oxygen profiles through the macular tissue are calculated by simulating the balance among oxygen supply, consumption and diffusion in: (a) physiological baseline conditions; (b) retinal blood flow reduced by 10%, 30% and 50% with respect to baseline; (c) choroidal oxygen level diminished by 10%, 30% and 50% with respect to baseline. Model simulations predict that: (1) the oxygenation of the foveal avascular zone is not affected by reduction in retinal blood flow; (2) a reduction in choroidal oxygen supply significantly affects the outer layers, especially the photoreceptors and outer nuclear layers; (3) the impact of reduction in choroidal oxygen supply is larger in the region more proximal to the macular center; (4) the impact of reduction in retinal blood flow is larger in the region more proximal to the macular periphery. The proposed mathematical model suggests that changes in retinal and choroidal oxygen supplies impact the oxygenation of the macular tissue differentially. These results may help better understand the pathogenesis of macular degeneration.

1. Introduction

Age-related macular degeneration (AMD) is the main cause of blindness in the developed world in subjects aged ≥ 55 years [1,2]. The prevalence of AMD in the U.S. is anticipated to increase to 22 million by the year 2050, and the global prevalence is expected to increase to 288 million by the year 2040 [1,2].

AMD can be classified as one of two types: dry (85% of cases) or wet (15% of cases), and aging represents the most important AMD risk factor [1–3]. As people age, acellular, polymorphous debris (formally

known as drusen) is deposited between the retinal pigment epithelium and Bruch's membrane [4]. The drusen may damage the retinal pigment epithelium (RPE), causing central vision distortion — known as dry AMD [2]. Dry AMD may convert to wet AMD, when chronic inflammation and hypoxia lead to aberrant vessel generation (choroidal neovascularization, CNV), with a rapid and severe vision loss [4,5].

Cigarette smoking, increased age, systemic vascular risk factors (such as cardiovascular disease, systemic arterial hypertension, elevated levels of systemic C-reactive protein), and fundus pigmentary anomalies (focal hyperpigmentation) have been recognized as risk

^{*} Correspondence to: Icahn School of Medicine at Mount Sinai, 1468 Madison Avenue, Annenberg 22-86, New York, NY 10029, United States of America. E-mail address: alon.harris@mssm.edu (A. Harris).

¹ MS, Ph.D., FARVO, Professor of Ophthalmology, Vice Chair of International Research and Academic Affairs, Director of the Ophthalmic Vascular Diagnostic and Research Program at Mount Sinai Hospital.

factors for progression to macular neovascularization (MNV) in patients with dry AMD [6–10]. However, the pathogenesis of the dry-to-wet conversion of AMD is still debated, and one of the conjectured causes is represented by an abnormal oxygenation in the macular tissue. The oxygen (O_2) supply to the macula is provided by two different sources, the retinal and choroidal vasculatures [11,12], and abnormalities in both circulations have been shown in patients with AMD using different imaging devices [13–18]. Therefore, both retinal and choroidal O_2 supplies may play a role in the dry-to-wet conversion of AMD through ischemia, but their relative importance is still not well understood.

Importantly, the diagnosis of MNV is traditionally made clinically when patients complain about visual symptoms and imaging devices such as optical coherence tomography (OCT), dye-based angiography, and OCT angiography (OCTA) show the evidence of fluid, leakage, or neovascular flow signal [5]. Interestingly, recent findings showed how OCTA may identify MNV without exudation in asymptomatic patients who present with dry maculae, defined as "nonexudative MNV" by the Classification of Atrophy consensus group [5].

In addition to this, it has been suggested that from a pathophysiological point of view the neovascularization in the case of non-exudative MNV may be beneficial, having the role of supporting the retinal pigment epithelium and outer retina. Therefore, the non-exudative MNV may represent a compensatory mechanism and not a pathologic process, at least initially, as reported in several clinical reports [5,19].

This work aims at clarifying the potential roles of retinal and choroidal O_2 supplies in AMD by means of a mathematical model that estimates the macular oxygenation on the basis of the physical mechanisms of O_2 transport, diffusion and consumption.

To achieve this goal, the model presented in this article adopts a two-dimensional description of the tissue in the macular region, thereby accounting for potential non-uniform O_2 distributions in both the longitudinal direction (i.e., along the retinal tissue layers) and the transversal direction (i.e., across the retinal thickness). This is a novelty of this article, with previous works assuming the O_2 distribution to be uniform in the longitudinal direction [20–22], or in the transversal direction [23], or both [24–26]. We note that a finite element analysis of retinal oxygenation has recently been presented in [27], but the work is focused on the influence of drusen rather than the relative influence of retinal and choroidal O_2 supplies.

The outline of the article is as follows. Section 2 illustrates the geometrical subdivision in layers of the macular region, the differential system that is proposed to mathematically describe the oxygenation process in the macula and the computational algorithm used to linearize and discretize the problem. Section 3 is devoted to discuss the results obtained by running the algorithm in the simulation of the oxygenation process under various biophysical conditions. The conclusive Section 4 collects the main findings of the research and indicates some future perspectives for knowledge advancement.

2. Mathematical model for macular oxygenation

The macular region is modeled as a layered structure including 7 layers: ganglion cell and nerve fiber layers (GCL), inner plexiform layer (IPL), inner nuclear layer (INL), outer plexiform layer (OPL), outer nuclear layer (ONL), inner segment of photoreceptors layer (PH), outer segments of photoreceptors and retinal pigmented epithelium (RPE). Each layer is characterized by specific levels of $\rm O_2$ consumption. Oxygen supply is provided by the vitreous and the choroid through the boundary conditions, and by three retinal capillary plexi, taken into account as volumetric source terms: superficial capillary plexus (SCP); intermediate capillary plexus (ICP); deep capillary plexus (DCP).

Table 1Thickness of the retinal layers and capillary plexi in parafoveal and foveal regions, derived from [28,29].

Retinal layer	Thickness (µm)	
	Parafoveal	Foveal
Retinal pigmented epithelium and outer	15	15
segment of photoreceptors		
Inner segment of photoreceptor layer	40	50
Outer nuclear layer	90	120
Outer plexiform layer	30	20
Inner nuclear layer	45	20
Inner plexiform layer	45	25
Ganglion cell and nerve fiber layer	70	20
Vascular plexus	Parafoveal	Foveal
Superficial capillary plexus	70	20
Intermediate capillary plexus	38	19
Deep capillary plexus	30	16

2.1. The simulation domain

Based on OCTA data reported in [28,29], the simulation domain considered in the present work is a two-dimensional region Ω : $\{\mathbf{x}=(x,z)\in(0,w_{ret})\times(0,t_{ret}(x))\}$ representing a cross-section of the macula. We note that, in this work, we focus on a two-dimensional analysis of the macular oxygenation in Ω , which should be seen as an important step towards more realistic three-dimensional simulations. The sequence of layers from the parafoveal region to the inner avascular zone is geometrically symmetric with respect to an axis located at the center $x=w_{ret}/2$ of the foveal avascular zone (FAZ). The boundary of the simulation domain is denoted by $\partial\Omega$ and is divided into three disjoint portions: the top boundary $\partial\Omega_{\rm vit}$ (at $z=t_{ret}(x)$, in contact with the vitreous), the bottom boundary $\partial\Omega_{\rm lat}$ (at x=0 and $x=w_{ret}$). We set $\Gamma_D:=\partial\Omega_{\rm vit}\cup\partial\Omega_{\rm ch}$ and we denote by $\mathbf{n}=\mathbf{n}(\mathbf{x})$ the outward unit normal vector on the domain boundary $\partial\Omega$.

The thickness of the retina is mathematically modeled by a sinusoidal function $t_{ret}=t_{ret}(x)$ which reaches a maximum of 335 µm in the parafoveal region and a minimum of 270 µm in the central macular region [28]. The width of the macular cross-section along the x-axis is equal to $w_{ret}=3$ mm and includes the region internal to the parafoveal annular zone, a fovea of 1 mm and a FAZ of 500 µm [38,39]. To obtain a realistic representation of the layers, their thickness in the parafoveal and in the foveal region has been retrieved from [28,29] and reported in Table 1. A transition region between the two regions has been modeled assuming a linear thinning of the layers towards the center. A similar approach has been used to treat the vascular layers. In particular, the DCP is considered to start in the middle of the OPL and the ICP at the two-thirds of the INL layer, whereas the SCP completely overlaps with the GCL layer.

2.2. The differential model

The process of O_2 delivery and diffusion to the retinal tissue geometrically described in Fig. 1 is mathematically modeled by the following nonlinear elliptic partial differential equation for the O_2 partial pressure $p = p(\mathbf{x})$, for any $\mathbf{x} \in \Omega$

$$\nabla \cdot (-D\nabla(\alpha p)) = S(\mathbf{x}, p). \tag{1}$$

The operator $\nabla = [\frac{\partial}{\partial x}, \frac{\partial}{\partial z}]^T$ represents the gradient with respect to Cartesian orthogonal coordinates, whereas the coefficients D and α represent tissue O_2 diffusivity and solubility, respectively. Numerical values and units for D and α are reported in Table 2. The function S on the right-hand side of Eq. (1) represents the net O_2 production rate in the retinal tissue and is mathematically expressed by a nonlinear

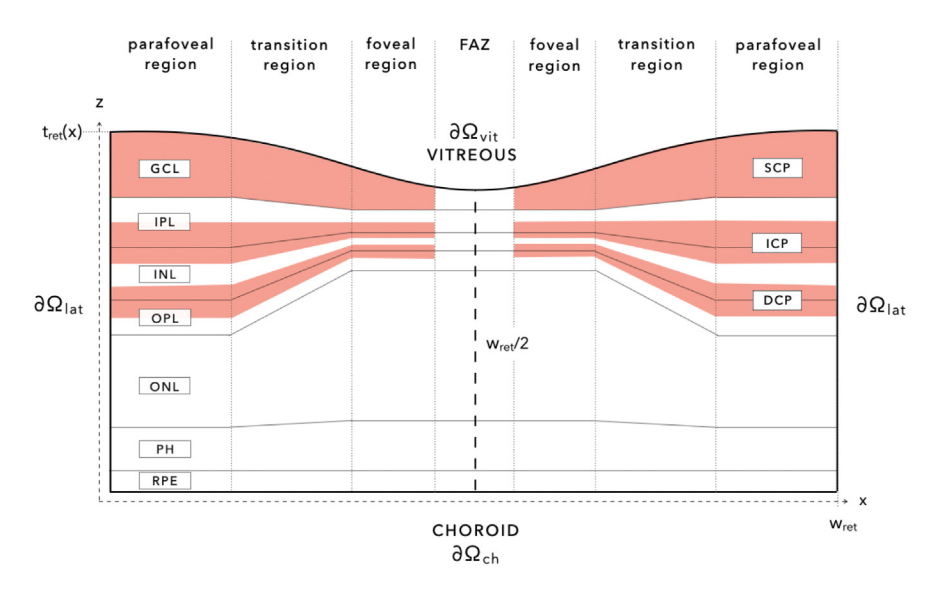


Fig. 1. The computational domain Ω and its partition into subregions. The inner retinal layers are: Ganglion Cell Layer, also comprising the nerve fiber layer, GCL; the Inner Plexiform Layer, IPL; the Inner Nuclear Layer, INL; the Outer Plexiform Layer, OPL. The outer retina is composed by: the Outer Nuclear Layer, ONL; the inner Plexiform Layer, IPL; the outer segments of photoreceptors and the Retinal Pigmented Epithelium, RPE. The pink color is used to identify the vascular regions: Superficial Capillary Plexus, SCP, Intermediate Capillary Plexus, ICP, and Deep Capillary Plexus, DCP.

Table 2Summary of model parameters. In the Units column the symbol "-" indicates a dimensionless quantity.

Parameter	Units	Value	Source
O_2 solubility, α	$ml_{O_2}ml^{-1}mmHg^{-1}$	$2.4 \cdot 10^{-5}$	[30]
O ₂ diffusivity, D	cm^2s^{-1}	1.4· 10 ⁻⁵	[31]
O_2 partial pressure at the vitreous, p_{vit}	mmHg	20	[21]
${\rm O}_2$ partial pressure at half maximum consumption $K_{1/2}$	mmHg	2	[32]
Maximum rate of O ₂ consumption:			
PH layer, Q_{OR}^{max}	mmHg s^{-1}	45	Adapted from [22,33]
RPE, ONL, Q_{OR}^{max}	$mmHg s^{-1}$	0	[21,22,33]
INL, outer segment of IPL,GCL, $Q_{\rm IR}^{\rm max}$	mmHg s ⁻¹	13	Adapted from [22,33]
OPL, inner segment of IPL, $Q_{\rm IR}^{\rm max}$	mmHg s^{-1}	26	Evaluated from [33,34]
O_2 capacity of red blood cells, c_o	$ml_{O_2} ml^{-1}$	0.5	[35]
Discharge hematocrit, H_D	-	0.4	[35]
Saturation drop in the capillary plexi:			
GCL, $\Delta S_{\rm sat}^{\rm GCL}$	-	0.09	Evaluated from [36]
ICP, $\Delta S_{\rm sat}^{\rm ICP}$	-	0.115	Evaluated from [36]
GCL, $\Delta S_{\rm sat}^{\rm DCP}$	-	0.194	Evaluated from [36]
Volume of GCL, $V_{ m GCL}$	cm ³	7.628 ·10 ⁻²	Evaluated from [36]
Volume of ICP, $V_{\rm ICP}$	cm ³	$3.269 \cdot 10^{-2}$	Evaluated from [36]
Volume of DCP, $V_{\rm DCP}$	cm ³	$3.269 \cdot 10^{-2}$	Evaluated from [36]
Healthy baseline O ₂ partial pressure			
at the choroid, $\overline{p}_{\mathrm{ch}}$	mmHg	80	[30]
Healthy baseline blood flow, \overline{Q}	ml s ⁻¹	$6.8178 \cdot 10^{-4}$	[37]

function of the O_2 partial pressure described in Section 2.3. The elliptic equation (1) is equipped with the following boundary conditions:

$$p(\mathbf{x}) = p_{\text{vit}}, \qquad \mathbf{x} \in \partial \Omega_{\text{vit}}, \qquad (2a)$$

$$p(\mathbf{x}) = p_{\rm ch} \qquad \mathbf{x} \in \partial \Omega_{\rm ch}, \tag{2b}$$

$$\nabla p(\mathbf{x}) \cdot \mathbf{n}(\mathbf{x}) = 0 \qquad \mathbf{x} \in \partial \Omega_{\text{lat}}, \tag{2c}$$

describing the facts that the levels of O_2 partial pressure at the macular boundary with the vitreous and the choroid are assumed to be given and equal to $p_{\rm vit}$ and $p_{\rm ch}$, respectively, (see Eq. (2a) and (2b)) and that no flux of oxygen is allowed to cross the lateral domain boundary

(see Eq. (2c)). The healthy baseline value of $p_{\rm ch}$ is assumed to be $\overline{p}_{\rm ch}=80$ mmHg. The value of $p_{\rm vit}$ is assumed to be equal to 20 mmHg.

2.3. Net production rate

The general expression of the right-hand side S of Eq. (1) reads

$$S = S(\mathbf{x}, p) = P(\mathbf{x}) - C(\mathbf{x}, p)$$
(3)

where the nonnegative function $P = P(\mathbf{x})$ accounts for the net O_2 supply provided by the capillary plexi within the macular layers, whereas the nonnegative function $C = C(\mathbf{x}, p)$, which depends nonlinearly on the

O₂ partial pressure, accounts for O₂ consumption by the metabolically active layers. Thus, S can be regarded as the net O2 production rate within the tissue. The characterization of the rates P and C strongly depends on the tissue layer:

$$P(\mathbf{x}) = \begin{cases} 0 & \mathbf{x} \in \text{layer } = \text{RPE, ONL, PH,OPL,INL,IPL,GCL} \\ G(\mathbf{x}) & \mathbf{x} \in \text{layer } = \text{DCP, ICP, GCL,} \end{cases}$$
(4a)

$$P(\mathbf{x}) = \begin{cases} 0 & \mathbf{x} \in \text{layer } = \text{RPE, ONL, PH,OPL,INL,IPL,GCL} \\ G(\mathbf{x}) & \mathbf{x} \in \text{layer } = \text{DCP, ICP, GCL,} \end{cases}$$

$$C(\mathbf{x}, p) = \begin{cases} 0 & \mathbf{x} \in \text{layer } = \text{RPE, ONL} \\ C_{\text{M-M}}(\mathbf{x}, p) & \mathbf{x} \in \text{layer } = \text{PH,OPL,INL,IPL,GCL,} \\ & \text{DCP, ICP, GCL.} \end{cases}$$

$$(4a)$$

The mathematical description of G and C_{M-M} is the object of the next two sections.

2.3.1. Production rate

The production rate $G = G(\mathbf{x})$ is described with the use of the Kroghtype cylinder model, as in [35,36]. In the regions where the capillary plexi are not present, the source term G is set equal to zero, while in the GCL, ICP and DCP layers the source term G is modeled as

$$G(\mathbf{x}) = c_0 H_D \frac{\Delta S_{\text{sat}}(\mathbf{x}) Q(\mathbf{x})}{V(\mathbf{x})}$$
 $\mathbf{x} \in \text{layer} = \text{DCP, ICP, GCL,}$ (5)

where $H_{\rm D}$ is the discharge hematocrit, $c_{\rm o}$ is the carrying capacity of red blood cells at 100% saturation, Q is the volumetric blood flow rate through the capillary plexi, $\Delta S_{\rm sat}$ is the saturation drop across the capillary plexi and V is the volume occupied by the capillary plexi. All the values of the parameters in (5) are reported in Table 2. We notice that ΔS_{sat} and V attain different values in each of the three plexi DCP, ICP and GCL. Following [36], we assume that the three capillary plexi are connected in series, so that the value of *O* is the same for all plexi. The value of Q in healthy conditions is assumed to be $\overline{Q} = 6.8178 \cdot 10^{-4}$ $ml s^{-1}$.

2.3.2. Consumption rate

Following [20], the consumption rate $C_{\mathrm{M-M}}$ is mathematically described via a Michaelis-Menten kinetics

$$C_{\mathrm{M-M}}(\mathbf{x},p) = \alpha \, \frac{Q^{\mathrm{max}}(\mathbf{x})p}{p + K_{1/2}}, \tag{6} \label{eq:cmm}$$

where $K_{1/2}$ and $Q^{\text{max}} = Q^{\text{max}}(\mathbf{x})$ represent the O_2 partial pressure at half maximum consumption and the maximum O2 consumption rate in the each layer, respectively. It is important to emphasize that the metabolic consumption is not uniformly distributed across the tissue layers, rather, Q^{max} is defined as a piecewise constant function of position, attaining a different constant value in each layer. The most relevant contribution occurs at the inner photoreceptors levels, in the outer retina (OR), and is denoted by $\mathcal{Q}_{\text{OR}}^{\text{max}}.$ In the inner retina (IR), the consumption rate is assumed to attain different values: the GCL, INL and the outer half of the IPL are characterized by the same maximum consumption rate as in [20], while the OPL and the inner part of the IPL are assumed to be highly metabolically active, with a value of $\mathcal{Q}_{\text{IR}}^{\text{max}}$ twice larger than in the other inner retinal layers. The different consumption levels have been adapted from [33,34]. All the parameters values and their units are reported in Table 2.

2.4. The algorithm

The nonlinear elliptic boundary value problem (1)- (2) is solved numerically by combining a fixed-point iteration method to linearize the nonlinear equation (1) (see Section 2.4.1) and a finite element approximation to discretize the resulting linearized boundary value problem (see Section 2.4.2). To better illustrate the method, it is convenient to rewrite the problem as follows:

$$\nabla \cdot (-D\nabla(\alpha p)) + c(\mathbf{x}, p(\mathbf{x})) p = P(\mathbf{x})$$
 in Ω , (7a)

$$p(\mathbf{x}) = p_{\text{vit}} \qquad \qquad \mathbf{x} \in \partial \Omega_{\text{vit}}, \tag{7b}$$

$$p(\mathbf{x}) = p_{\rm ch} \qquad \qquad \mathbf{x} \in \partial \Omega_{\rm ch}, \tag{7c}$$

$$\nabla p(\mathbf{x}) \cdot \mathbf{n}(\mathbf{x}) = 0 \qquad \qquad \mathbf{x} \in \partial \Omega_{\text{lat}}, \tag{7d}$$

where

$$c\left(\mathbf{x}, p(\mathbf{x})\right) = \begin{cases} 0 & \mathbf{x} \in \text{layer } = \text{RPE, ONL} \\ \frac{\alpha \mathcal{Q}^{\max}(\mathbf{x})}{p(\mathbf{x}) + K_{1/2}} & \mathbf{x} \in \text{layer } = \text{PH,OPL,INL,IPL,GCL, DCP, ICP.} \end{cases}$$

We denote by $p_D: \Gamma_D \to \mathbb{R}$ the positive function such that $p_D|_{\partial\Omega_{\mathrm{vir}}} =$ p_{vit} and $p_D|_{\partial\Omega_{\text{ch}}} = p_{\text{ch}}$, and we denote by $\mathcal{R}p_D: \Omega \to \mathbb{R}$ any positive function of $H^1(\Omega)$ such that $\mathcal{R}p_D|_{\Gamma_D} = p_D$. Let $\mathcal{V} =$ $\left\{\phi \in H^1(\Omega) \, | \, \phi|_{\Gamma_D} = 0 \right\}$. The weak formulation of the nonlinear prob-

find p, with $(p - \mathcal{R}p_D) \in \mathcal{V}$, such that

$$\int_{\Omega} D\nabla(\alpha p) \cdot \nabla \phi \, d\Omega + \int_{\Omega} c(\mathbf{x}, p) p \phi \, d\Omega = \int_{\Omega} P \phi \, d\Omega \qquad \forall \phi \in \mathcal{V}. \tag{9}$$

2.4.1. The fixed-point map

For a given function $v \in H^1(\Omega)$ such that v > 0 almost everywhere (a.e.) in Ω and $(v - \mathcal{R}p_D) \in \mathcal{V}$, we define the abstract operator T: $H^1(\Omega) \to H^1(\Omega)$ by letting

$$u = T(v) \tag{10}$$

be the unique weak solution of the following linear reaction-diffusion boundary value problem:

$$\nabla \cdot (-D\nabla(\alpha u)) + c(\mathbf{x}, v(\mathbf{x}))u = P(\mathbf{x}) \qquad \text{in } \Omega, \tag{11a}$$

$$u(\mathbf{x}) = p_{\text{vit}} \qquad \qquad \mathbf{x} \in \partial \Omega_{\text{vit}}, \tag{11b}$$

$$u(\mathbf{x}) = p_{\rm ch}$$
 $\mathbf{x} \in \partial \Omega_{\rm ch}$, (11c)

$$\nabla u(\mathbf{x}) \cdot \mathbf{n}(\mathbf{x}) = 0 \qquad \qquad \mathbf{x} \in \partial \Omega_{\text{lat}}. \tag{11d}$$

Let $p^{(0)} \in H^1(\Omega)$ such that p > 0 a.e. in Ω and $(p^{(0)} - \mathcal{R}p_D) \in \mathcal{V}$. For $j \ge 0$ until convergence, the fixed-point iteration computes $p^{(j)}$ through the abstract recursive formula

$$p^{(j+1)} = T(p^{(j)}). (12)$$

The above recursive relation amounts to solving at each step $i \ge 0$ the following linear reaction-diffusion boundary value problem:

$$\nabla \cdot (-D\nabla(\alpha p^{(j+1)})) + c(\mathbf{x}, p^{(j)}(\mathbf{x}))p^{(j+1)} = P \qquad \text{in } \Omega$$
 (13a)

$$p^{(j+1)}(\mathbf{x}) = p_{\text{vit}} \qquad \qquad \mathbf{x} \in \partial \Omega_{\text{vit}}, \tag{13b}$$

$$p^{(j+1)}(\mathbf{x}) = p_{\text{ch}} \qquad \mathbf{x} \in \partial \Omega_{\text{ch}}, \tag{13c}$$

$$\nabla p^{(j+1)}(\mathbf{x}) \cdot \mathbf{n}(\mathbf{x}) = 0 \qquad \qquad \mathbf{x} \in \partial \Omega_{\text{lat}}. \tag{13d}$$

2.4.2. Finite element approximation

Besides being nonlinear, another challenging property of the elliptic boundary value problem (1)- (2) is the heterogeneity of the production and consumption rates P and c. This means, in particular, that both gand c may be discontinuous functions across the various retinal layers, according to the definitions (4). An efficient and flexible manner to numerically deal with the heterogeneity of P and c is to use the Finite Element Method (FEM) to approximate the solution of the linearized equation (13a) for each $j \ge 0$ until convergence (see [40, Chapters 5-6]). To this purpose, the FEM with piecewise linear basis functions has been used to solve the linearized model illustrated in Section 2.4.1 within the framework of the open source software Freefem++ on an unstructured triangulation \mathcal{T}_h of the domain $\overline{\Omega}$, h > 0 being the socalled discretization parameter representing a measure of the diameter of the triangles in \mathcal{T}_h (see [36] and [41]). The fixed-point iteration (12) is terminated at the first value $j^* \ge 0$ of the iteration counter such that the following stopping criterion is satisfied

$$\frac{\|p_h^{(j^*+1)} - p_h^{(j^*)}\|_{L^2(\Omega)}}{\|p_h^{(j^*+1)}\|_{L^2(\Omega)}} < \varepsilon \tag{14}$$

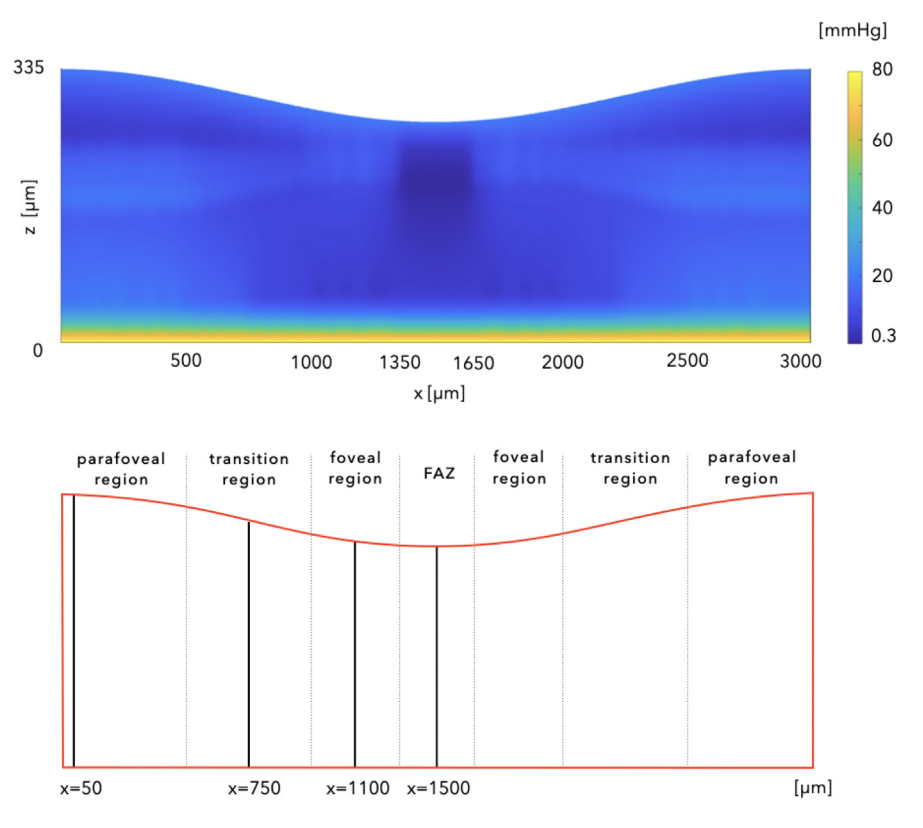


Fig. 2. Top panel: color map of the spatial distribution of model predicted O_2 partial pressure over the macular region in baseline conditions. Bottom panel: macular domain where the four coordinates along the x-axis, $x = 50, 750, 1100, 1500 \,\mu\text{m}$, have been identified for the analysis of simulation results.

where for all $\phi \in L^2(\Omega)$ we let $\|\phi\|_{L^2(\Omega)} = \left(\int_{\Omega} \phi^2(\mathbf{x}) d\Omega\right)^{1/2}$, whereas p_h denotes the finite element approximation of the O₂ partial pressure p and ε is a user-specified tolerance. In the numerical simulations illustrated in Section 3 we have set $\varepsilon = 10^{-6}$.

3. Results

The model and computational algorithm described in Section 2 are used to perform simulations in the following three different scenarios of clinical interest:

- **1. healthy baseline conditions,** where retinal blood flow and choroidal partial pressure of oxygen are assumed to be at their baseline values, namely $Q = \overline{Q}$ and $p_{\rm ch} = \overline{p}_{\rm ch}$;
- **2. reduced retinal blood flow,** where Q is reduced by 10%, 30% and 50% with respect to baseline while the O_2 choroidal partial pressure remains unaltered;
- **3. reduced choroidal oxygen supply,** where $p_{\rm ch}$ is reduced by 10%, 30% and 50% with respect to baseline while Q remains unaltered.

Scenarios 2 and 3 represent two different pathological conditions that may impair macular oxygenation, namely reduced retinal and choroidal O_2 supplies, respectively. From the mathematical perspective, these scenarios differ by the type of source terms that are impaired, namely volumetric sources in the case of O_2 supplied by the retina (Scenario 2) and boundary sources in the case of O_2 supplied by the choroid (Scenario 3). Note that the values assumed for reduction of blood flow in pathological conditions appear to be in agreement with data reported in Pappelis et al. [42]. In all simulations we have set $\rho_{\text{vit}} = 20$ mmHg and we have taken the initial O_2 spatial distribution $\rho_h^{(0)}$ as the linear interpolant of the Dirichlet boundary conditions. Moreover, the number of iterations to satisfy the stopping criterion (14) has shown to

vary between 30 (Scenario 2, reduction of Q by 50% with respect to baseline) and 46 (healthy case and Scenario 3, reduction of $p_{\rm ch}$ by 10% with respect to baseline).

Fig. 2 (top panel) illustrates the colormap of the spatial distribution of O_2 partial pressure over the whole macular region predicted by the model in baseline conditions. Fig. 3 shows the 2D colormaps of the source term $P(\mathbf{x})$ related to retinal circulation oxygen delivery (Panel A) and the consumption term $C(\mathbf{x})$, specific of each retinal tissue and nonlinear with respect to the available partial pressure of oxygen (Panel B). Results show that far from the avascular region, O_2 partial pressure in the inner retina is predicted to lie in the range $10-20 \, \text{mmHg}$, in agreement with O_2 partial pressure data reported in [43].

Fig. 2 (bottom panel) provides a schematic representation of the macular domain where four coordinates along the x-axis, x=50, 750, 1100, 1500 μ m, have been identified for the analysis of simulation results. Fig. 4 shows the predicted O_2 partial pressure profiles in correspondence of these four x-coordinates. Each of the four oxygen partial pressure distributions shows some common features:

- a steep decrease of the partial pressure of oxygen from the choroid until the PH layer, related to the high metabolic consumption of photoreceptors;
- a plateau-like behavior in the remaining part of the outer retina.

This general behavior can also be observed in rhesus monkey, cat and rat retinas, as reported in the experimental data of [43]. In this latter work, the authors observed the presence of a local minimum of oxygen concentration in the IPL, which is also exhibited by our simulations pertaining to the parafoveal, transition and foveal regions reported in the top and bottom left panels of Fig. 2. It is interesting to notice that the steep decrease in the PH layer does also correspond to the minimum value attained by the partial pressure of oxygen in the foveal region. In addition, our simulations also reveal a local increase of oxygen partial pressure in the vascularized regions of the OPL, correlated to the presence of DCP, a behavior that is no longer observable as one

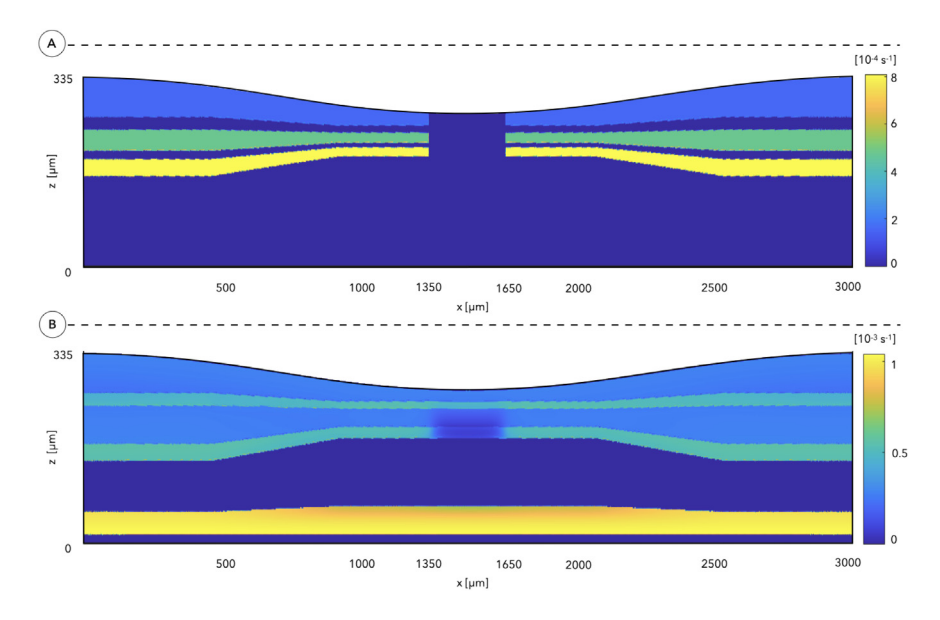


Fig. 3. Panel A: color map of the spatial distribution of model predicted source term $P(\mathbf{x})$ over the macular region in baseline conditions. Panel B: color map of the spatial distribution of model predicted non linear consumption term $C(\mathbf{x})$ over the macular region in baseline conditions.

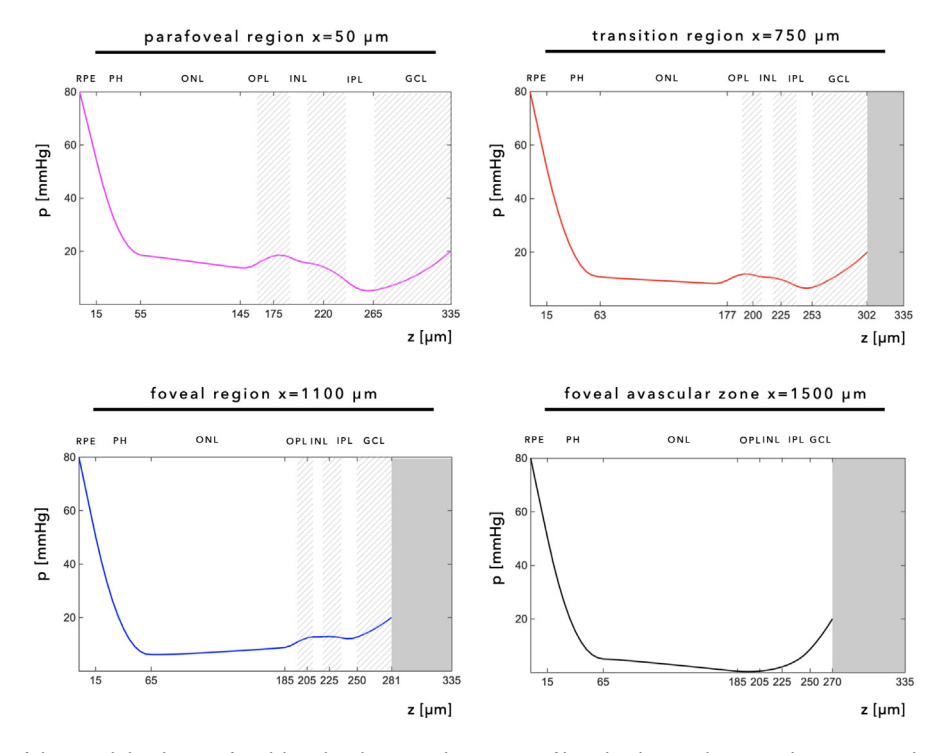


Fig. 4. Cross-sectional views of the spatial distribution of model predicted O_2 partial pressure profile in baseline conditions. Each cross-sectional view corresponds to one of the four coordinates identified in Fig. 2. The shaded regions highlight the presence of the vascular regions. The darker shaded region corresponds to the end of the retina.

approaches the FAZ. As a matter of fact, in Fig. 4 (bottom right panel) the local increase completely disappears, and, instead, we observe a continuous reduction of the oxygen partial pressure moving towards the IPL, the minimum value being attained in correspondence of the OPL.

Figs. 5 and 6 show the O_2 partial pressure across the retinal thickness in Scenario 2 and 3 whereas Figs. 7 and 8 illustrate the model predicted relative difference in the O_2 partial pressure (%) between Scenario 2 and Scenario 1, and between Scenario 3 and Scenario 1, respectively. The relative pressure differences have been computed across the macular thickness in the parafoveal and transition regions (top row of Figs. 7 and 8) and across the foveal region and the foveal avascular zone (bottom row of Figs. 7 and 8). The relative pressure

difference has been computed as

$$\Delta p = \frac{p_I - p_H}{p_H} \%,\tag{15}$$

where p_I is the partial pressure of oxygen obtained from either Scenario 2 or 3 modeling an impaired vascular condition, whereas p_H is the partial pressure of oxygen obtained from Scenario 1, with healthy baseline conditions.

Model simulations predict that:

1 the impact of reduction in retinal blood flow is larger in the region more proximal to the macular periphery (see Fig. 7);

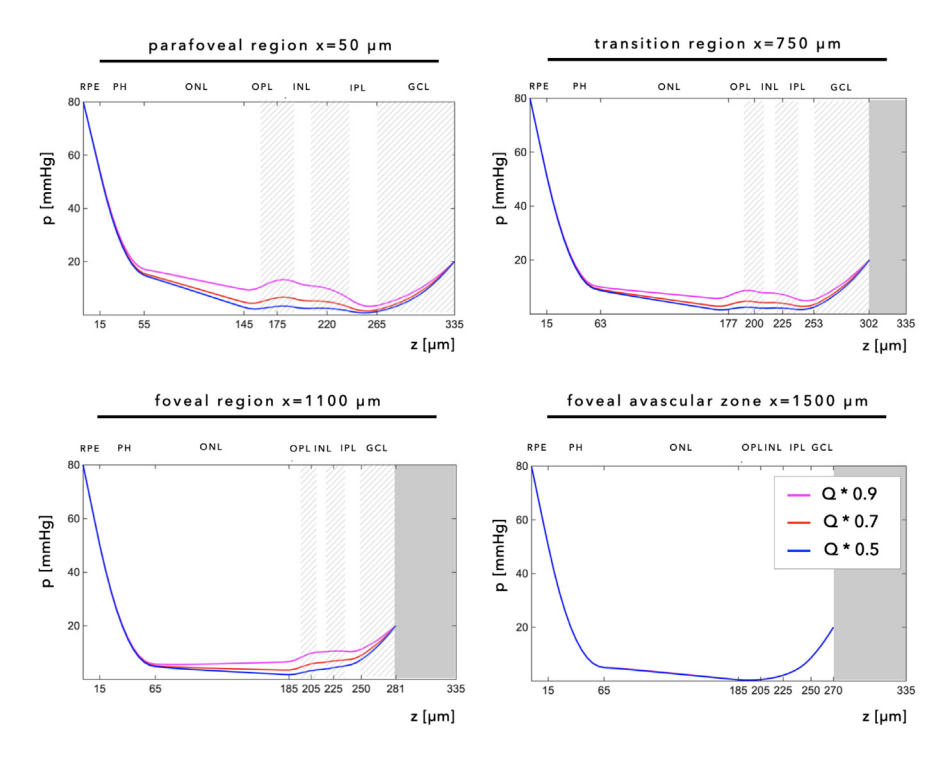


Fig. 5. Model predicted relative O₂ partial pressure (mmHg) in Scenario 2 across the macular thickness in the parafoveal region (top row, left panel), the transition region (top row, right panel), the foveal region (bottom row, left panel) and foveal avascular zone (bottom row, right panel). The shaded regions highlight the presence of the vascular regions. The darker shaded region corresponds to the end of the retina.

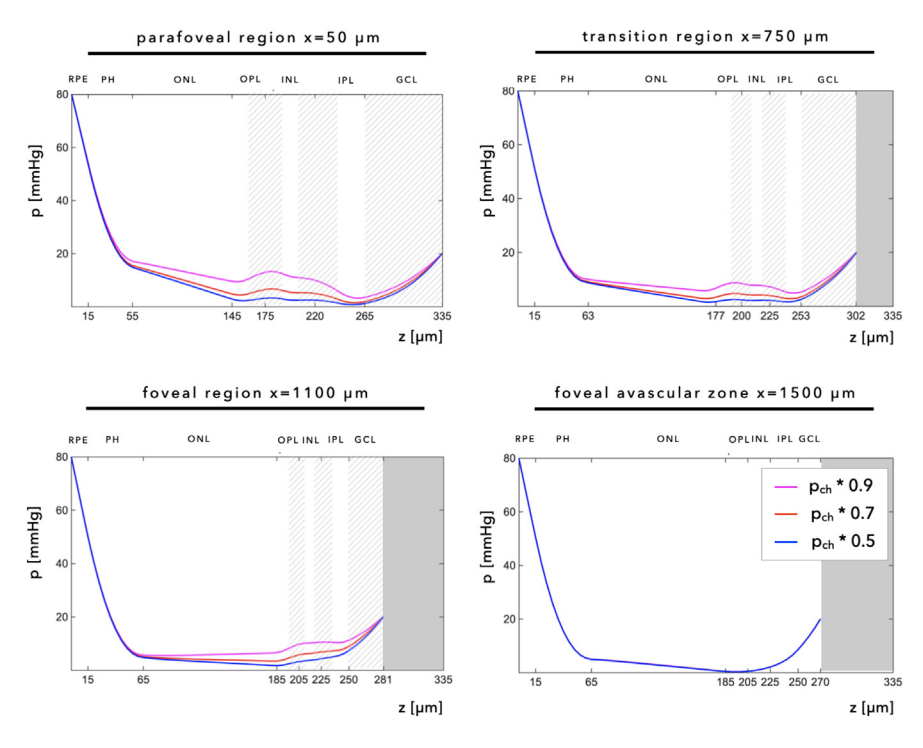


Fig. 6. Model predicted relative O₂ partial pressure (mmHg) in Scenario 3 across the macular thickness in the parafoveal region (top row, left panel), the transition region (top row, right panel), the foveal region (bottom row, left panel) and foveal avascular zone (bottom row, right panel). The shaded regions highlight the presence of the vascular regions. The darker shaded region corresponds to the end of the retina.

- 2 the oxygenation of the foveal avascular zone is not markedly affected by reduction in retinal blood flow (see Fig. 7, right column, bottom row).
- 3 a reduction in choroidal oxygen supply is affecting mostly the outer layers, especially the photoreceptors and outer nuclear layers (see Fig. 8);
- 4 the impact of reduction in choroidal oxygen supply is larger in the region more proximal to the macular center (see Fig. 8).

Let us further elaborate on the implications of these results, which suggest that impairment in choroidal and retinal O_2 supplies may have a different impact on the oxygenation of the macular tissue depending on the specific tissue layer and on the distance from the macula

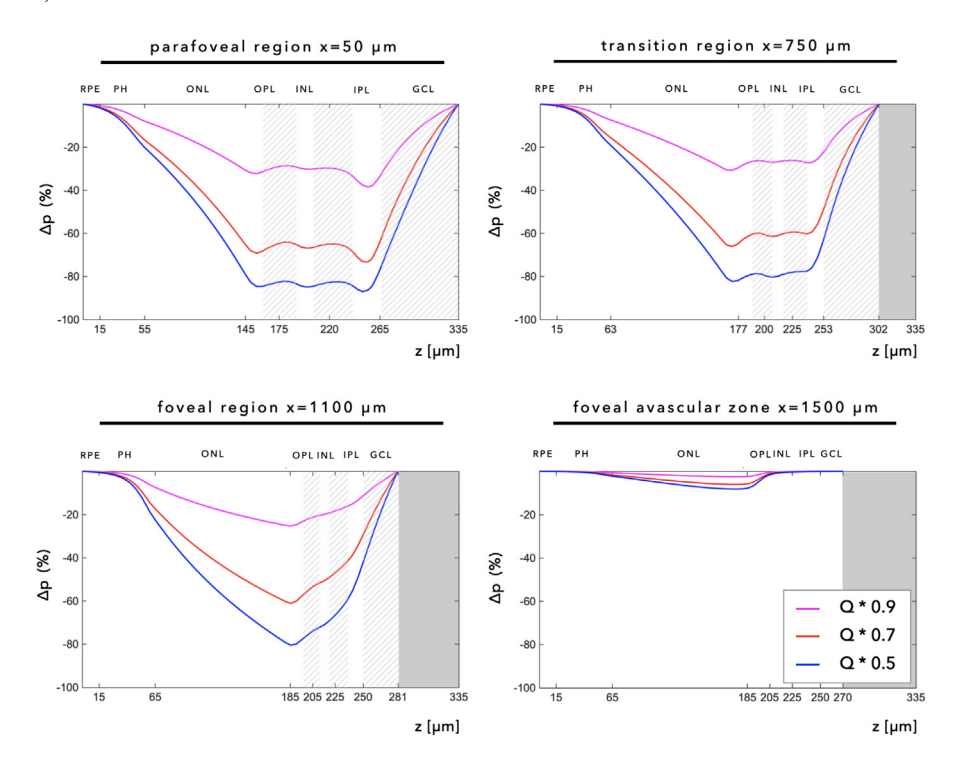


Fig. 7. Model predicted relative difference in the O_2 partial pressure (%) between Scenario 2 and Scenario 1 across the macular thickness in the parafoveal region (top row, left panel), the transition region (top row, right panel), the foveal region (bottom row, left panel) and foveal avascular zone (bottom row, right panel). The shaded regions highlight the presence of the vascular regions. The darker shaded region corresponds to the end of the retina.

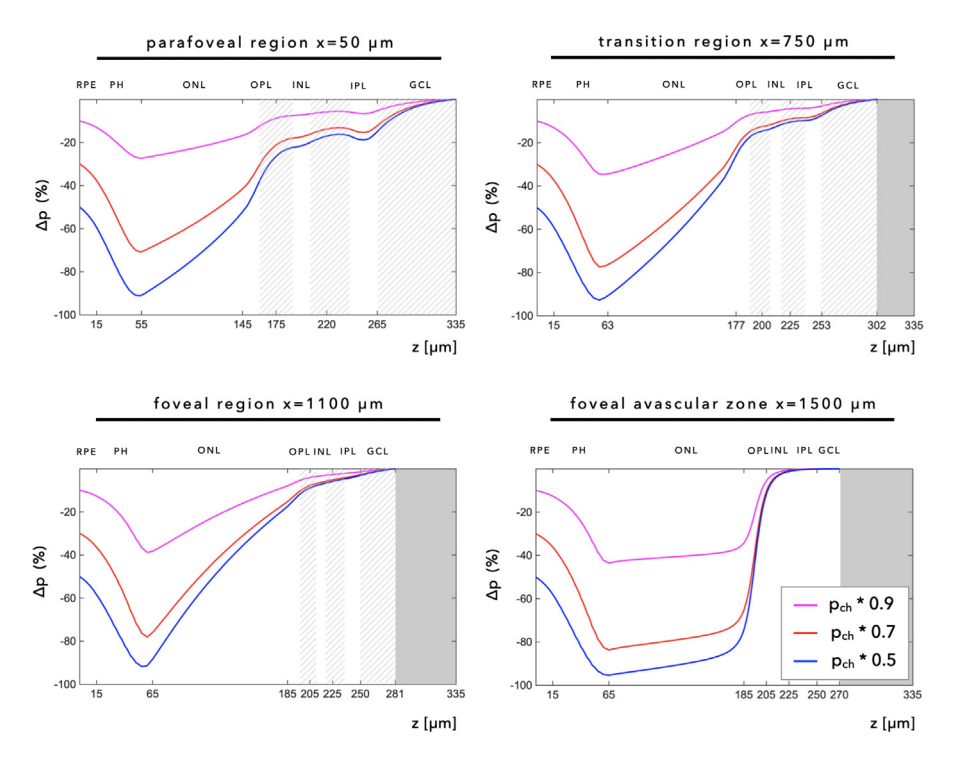


Fig. 8. Model predicted relative difference in the O_2 partial pressure (%) between Scenario 3 and Scenario 1 across the macular thickness in the parafoveal region (top row, left panel), the transition region (top row, right panel), the foveal region (bottom row, left panel) and foveal avascular zone (bottom row, right panel). The shaded regions highlight the presence of the vascular regions. The darker shaded region corresponds to the end of the retina.

(center or periphery). Specifically, our results show that the retinal contribution to the oxygenation of the avascular region of the macula is marginal, while it plays a major role in the internal layers of other

macular regions. As shown in Fig. 7, a decrease in retinal blood flow mainly affects the layers close to the capillary plexi (denoted by the striped pattern), but only in the parafoveal and in the transition zone. In

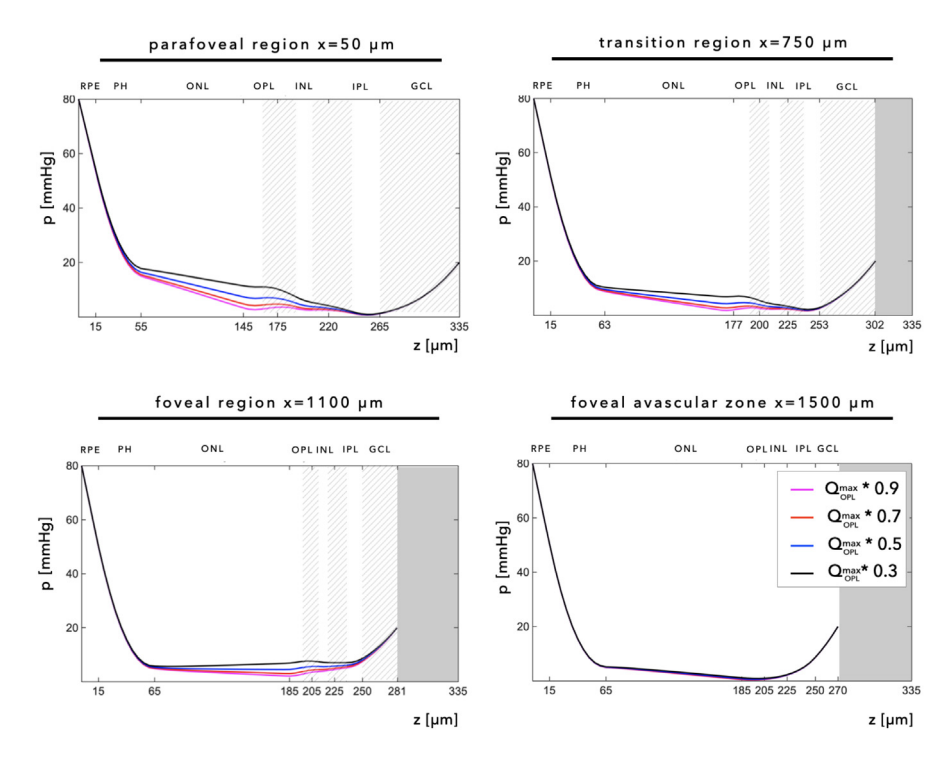


Fig. 9. Model predicted O_2 partial pressure (mmHg) profile with reduced maximum oxygen consumption in the Outer Plexiform layer and 50% reduction of retinal blood flow across the macular thickness in the parafoveal region (top row, left panel), the transition region (top row, right panel), the foveal region (bottom row, left panel) and foveal avascular zone (bottom row, right panel). The shaded regions highlight the presence of the vascular regions. The darker shaded region corresponds to the end of the retina.

support to this consideration, we see that in the FAZ, which is capillary free, the relative difference is almost null.

In the parafoveal region up to the foveal region, the choroid seems to be the main $\rm O_2$ supplier of the outer layers, namely the layer of the photoreceptors, which plays a crucial role in the physiology of vision and has the highest metabolic consumption of oxygen in the whole retinal tissue (Fig. 8). By contrast, the oxygenation in the middle and inner layers does not seem to be markedly influenced by the choroidal supply. In the FAZ instead, the choroid seems to play a major role in the oxygenation not only of the photoreceptors layer, but also of the outer nuclear layer and outer plexiform layer (Fig. 8, right column, bottom row). In the FAZ, the oxygenation of the most internal layers (inner plexiform layer, and ganglion cell and nerve fiber layer), seems to depend on the partial pressure of oxygen supplied by the vitreous.

In light of these results, in the vascularized regions of the macula, retinal $\rm O_2$ supply seems to be responsible for the nourishment of the middle-internal layers (outer plexiform layer, inner nuclear layer, inner plexiform layer), while the choroid seems mainly responsible for the nourishment of the photoreceptors layer, to which it is spatially close. A different consideration should be made for the FAZ: retinal circulation does not seem to play any role in the supply of oxygen of the central avascular macular region, whereas the choroid is suggested to be the main oxygen source for all photoreceptors layers, outer nuclear layer, outer plexiform layer, and, marginally, for the inner nuclear layer.

It is worth mentioning that retinal blood flow reductions may be involved in the pathophysiology of other ocular diseases besides AMD. A major example is glaucoma, where a dysfunctional behavior of the retinal vasculature has been observed in many studies, as reviewed in [44]. The proposed mathematical modeling approach may be particularly useful in investigating potential vascular factors involved in other vascular beds of the eye, including those supplying the optic nerve, to further investigate visual field losses in glaucoma (see [45–47]).

Regulation of oxygen extraction. In the performed simulations of pathological scenarios reported so far, the value of several parameters has been kept equal to the value in healthy baseline condition. This choice is consistent with lack of experimental data in the considered situations. Indeed, future quantitative estimation would strongly benefit of ad-hoc experimentally measured parameters.

Despite the difficulties in retrieving reasonable data on the considered physiological conditions, in order to investigate the possible effects of regulation of oxygen extraction on predicted macula oxygenation we have performed the simulations in the worst cases of Scenarios 2 and 3 by reducing the maximum oxygen consumption \mathcal{Q}_{IR}^{max} in the OPL layer. The parametric analysis of this condition is indeed supported by previous studies [33] where the OPL has been shown to modify its consumption rate in regime of hypoxia. In the present work, the parametric study is conducted in the case of 50% reduction of retinal blood flow (Fig. 9) and 50% reduction in the choroidal partial pressure of oxygen (Fig. 10).

The results reported in Figs. 9 and 10 show how the ability of OPL in reducing its oxygen consumption is more incisive when the choroidal perfusion is impaired, whereas it plays a less relevant role when the retinal circulation is affected. Consistently, the major effects are observable in the proximity of the OPL layer. The FAZ, in both scenarios, remains unaltered by the regulative variation of oxygen consumption of the OPL.

The role of the vitreous. After having discussed the role of retinal and choroidal circulation in the delivery of oxygen to the retina, we now consider the possible occurrence of a noncompletely efficient exchange of oxygen with the vitreous compartment. In doing so, we replace the Dirichlet boundary condition at the interface between retina and vitreous with the following Robin boundary condition

$$J(\mathbf{x}) \cdot \mathbf{n}(\mathbf{x}) = -k_{vit}(p_{vit} - p(\mathbf{x})) \qquad \mathbf{x} \in \partial \Omega_{vit}$$
(16)

where:

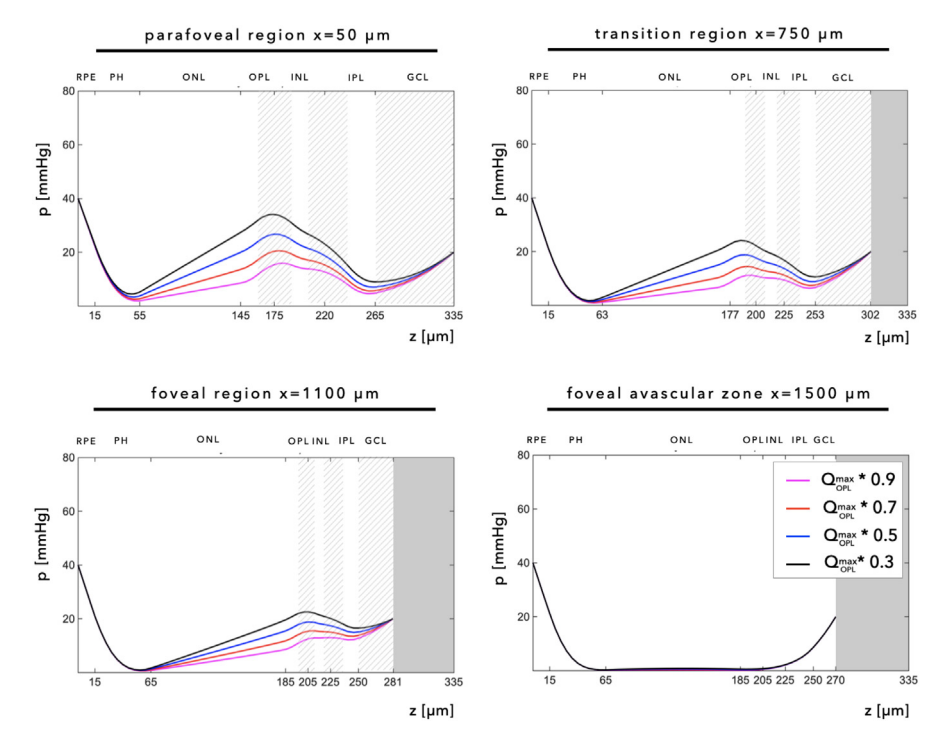


Fig. 10. Model predicted O₂ partial pressure (mmHg) profile with reduced maximum oxygen consumption in the Outer Plexiform layer and 50% reduction of choroidal partial pressure across the macular thickness in the parafoveal region (top row, left panel), the transition region (top row, right panel), the foveal region (bottom row, left panel) and foveal avascular zone (bottom row, right panel). The shaded regions highlight the presence of the vascular regions. The darker shaded region corresponds to the end of the retina.

- 1. $J(\mathbf{x}) \cdot \mathbf{n}(\mathbf{x})$ is the normal component of the oxygen flux density at any $\mathbf{x} \in \partial \Omega_{\text{vit}}$ (cm s⁻¹);
- 2. p_{vit} is the (given) value of the oxygen partial pressure in the vitreous region (mmHg);
- 3. $p(\mathbf{x})$ is the oxygen partial pressure at any $\mathbf{x} \in \partial \Omega_{\text{vit}}$ (mmHg);
- 4. $k_{vit} \geq 0$ is a parameter which effectively describes the efficiency of exchange of oxygen across the retina-vitreous interface (cm s⁻¹ mmHg⁻¹).

Note that setting $k_{vit} = +\infty$ into (16) degenerates into

$$p(\mathbf{x}) = p_{vit} \qquad \mathbf{x} \in \partial \Omega_{vit} \tag{17}$$

which corresponds to the Dirichlet boundary condition (2a) implemented in all the simulations illustrated so far. The predicted relative difference in the $\rm O_2$ partial pressure (%) reported in Figure 11 has been computed as

$$\Delta p = \frac{p_R - p_D}{p_D}\%,\tag{18}$$

where p_R is the partial pressure of oxygen computed by imposing the Robin boundary condition (16) with various values of k_{vit} , while p_D is the partial pressure of oxygen computed in healthy conditions by imposing the Dirichlet boundary condition (17).

Simulations have been performed for different values of k_{vit} , ranging from 10^2 to $0~{\rm cm\,s^{-1}}$ mmHg $^{-1}$. Note that assuming $k_{vit}=0~{\rm cm\,s^{-1}}$ mmHg $^{-1}$ is physiologically equivalent to assuming that the vitreous does not contribute at all to the oxygenation of the inner layers of the retina, thus reflecting the worst possible physiological condition. The results reported in Fig. 11 show how switching off the interplay between the vitreous and the macular tissue negligibly affects the PH layer, even in the worst case with $k_{vit}=0~{\rm cm\,s^{-1}}\,{\rm mmHg^{-1}}$. Instead, the inner layers, particularly in the FAZ, undergo a major effect. The IPL layer, in particular, appears to be strongly affected by a possible decrease in the efficiency of exchange of oxygen with the vitreous region.

4. Conclusions

With an increasing number of studies implicating blood flow as an important factor in the etiology and progression of AMD [13–15], it is imperative to understand the relationship between the retinal and choroidal contributions to macular oxygenation. As a matter of fact, the role of the retinal capillary plexi is still controversial, but crucial to gain further understanding of the pathophysiology of macular diseases with a high epidemiologic impact worldwide, such as AMD [1,2]. In this work, we utilized a novel mathematical model to help shed light on these important issues.

To the best of our knowledge this represents the first study of applied physics-based mathematical modeling to characterize how abnormalities in the retinal and choroidal O₂ supplies may affect macular oxygenation in different retinal layers and at various distances from the macula. Specifically, our results suggest that the center of the macula appears to be more affected by changes in the choroidal circulation, while the periphery is more affected by variations in retinal blood flow. Additionally, the outer layers of the retina seem to be mostly affected by a reduction in the choroidal oxygen supply. Interestingly, the presented model supports the new insights in the natural history and progression of neovascular AMD, suggesting that AMD progresses from non-neovascular forms to non-exudative neovascular forms (with type 1 MNV, beneath the RPE and its basal lamina, compensating for choroidal ischemia to support the RPE and outer retina) to exudative neovascular forms (perhaps with over-proliferation of type 1 MNV and subsequent leakage and/or conversion of type 1 to type 2 MNV, above the RPE) [5]. Importantly, the concept of non-exudative neovascular AMD and its beneficial role in the disease progression has been reported in several clinical pathologic reports [5,19], and the results from our model are consistent with such findings. These insights may be further coupled with mathematical models of ocular hemodynamics [12,37] and used to enhance artificial intelligence (AI) methods for data analysis in ophthalmology [11,48] to aid the design of personalized approaches to AMD management, as our group has recently described in glaucoma [49].

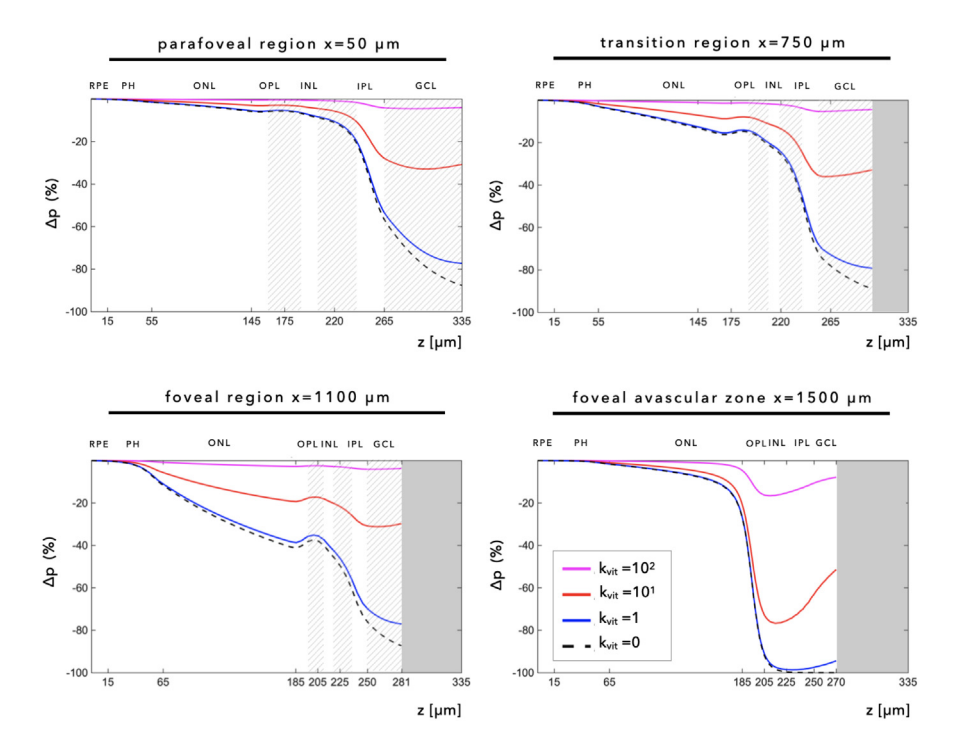


Fig. 11. Model predicted relative difference in the O₂ partial pressure (%) between a scenario with the Robin boundary condition (16) and the case with the Dirichlet boundary condition (17). The relative differences have been computed across the macular thickness in the parafoveal region (top row, left panel), the transition region (top row, right panel), the foveal region (bottom row, left panel) and foveal avascular zone (bottom row, right panel). The shaded regions highlight the presence of the vascular regions. The darker shaded region corresponds to the end of the retina.

Synopsis. Macular oxygenation is differentially affected by abnormalities in the oxygen supplied by the choroid and the retinal circulation.

Fundings

This work was supported by NIH grant R01EY030851 (Alon Harris), NSF DMS 1853222/2021192 (Giovanna Guidoboni and Alon Harris), a Challenge Grant award from Research to Prevent Blindness, NY (Alon Harris).

Declaration of competing interest

The Authors declare that there is no conflict of interest. Professor A. Harris would like to disclose that he received remuneration from AdOM, Qlaris, Luseed, and Cipla for serving as a consultant, and he serves on the board of AdOM, Qlaris, and Phileas Pharma. Professor A. Harris holds an ownership interest in AdOM, Luseed, Oxymap, Qlaris, Phileas Pharma, and QuLent. All relationships listed above are pursuant to Icahn School of Medicine's policy on outside activities. Dr. G. Guidoboni would like to disclose that she received remuneration from Foresite Healthcare LLC for serving as a consultant. Dr. G. Guidoboni holds an ownership interest in Gspace LLC.

References

- [1] A. García-Layana, F. Cabrera-López, J. García-Arumí, L. Arias-Barquet, J.M. Ruiz-Moreno, Early and intermediate age-related macular degeneration: Update and clinical review, Clin. Interv. Aging 12 (2017) 1579–1587, http://dx.doi.org/10. 2147/CIA.S142685.
- [2] K.L. Pennington, M.M. DeAngelis, Epidemiology of age-related macular degeneration (AMD): associations with cardiovascular disease phenotypes and lipid factors, Eye and Vision 3 (1) (2016) 1–20, http://dx.doi.org/10.1186/s40662-016-0063-5, URL: http://dx.doi.org/10.1186/s40662-016-0063-5.
- [3] I. Bhutto, G. Lutty, Understanding age-related macular degeneration (AMD): Relationships between the photoreceptor/retinal pigment epithelium/Bruch's membrane/choriocapillaris complex, Mol. Aspects Med. 33 (4) (2012) 295–317, http://dx.doi.org/10.1016/j.mam.2012.04.005, URL: http://dx.doi.org/10.1016/j.mam.2012.04.005.

- [4] M. Van Lookeren Campagne, J. Lecouter, B.L. Yaspan, W. Ye, Mechanisms of age-related macular degeneration and therapeutic opportunities, J. Pathol. 232 (2) (2014) 151–164. http://dx.doi.org/10.1002/path.4266.
- [5] L. Chen, M. Li, J. Messinger, D. Ferrara, C. Curcio, K. Freund, Recognizing atrophy and mixed-type neovascularization in age-related macular degeneration via clinicopathologic correlation, Transl. Vision Sci. Technol. 9,8 (2020) http: //dx.doi.org/10.1167/tvst.9.8.8.
- [6] The Complications of Age-related Macualar Degeneration Prevention Trial (CAPT) Research Group, Risk factors for choroidal neovascularization and geographic atrophy in the complications of age-related macular degeneration prevention trial, in: Ophthalmology, 115, (9) Complications of Age-related Macular Degeneration Prevention Trial (CAPT) Research Group, 2008, http: //dx.doi.org/10.1016/j.ophtha.2008.03.008.
- [7] R.E. Hogg, J.V. Woodside, S.E. Gilchrist, R. Graydon, A.E. Fletcher, W. Chan, A. Knox, B. Cartmill, U. Chakravarthy, Cardiovascular disease and hypertension are strong risk factors for choroidal neovascularization, Ophthalmology 115 (6) (2008) http://dx.doi.org/10.1016/j.ophtha.2007.07.031.
- [8] M. Kikuchi, M. Nakamura, K. Ishikawa, T. Suzuki, H. Nishihara, T. Yamakoshi, K. Nishio, K. Taki, T. Niwa, N. Hamajima, H. Terasaki, Elevated C-reactive protein levels in patients with polypoidal choroidal vasculopathy and patients with neovascular age-related macular degeneration, Ophthalmology 114 (9) (2007) 1722–1727, http://dx.doi.org/10.1016/j.ophtha.2006.12.021.
- [9] U. Chakravarthy, T.Y. Wong, A. Fletcher, E. Piault, C. Evans, G. Zlateva, R. Buggage, A. Pleil, P. Mitchell, Clinical risk factors for age-related macular degeneration: A systematic review and meta-analysis, BMC Ophthalmology 10 (1) (2010) http://dx.doi.org/10.1186/1471-2415-10-31.
- [10] J.S. Tan, P. Mitchell, W. Smith, J.J. Wang, Cardiovascular risk factors and the long-term incidence of age-related macular degeneration. The blue mountains eye study, Ophthalmology 114 (6) (2007) 1143–1150, http://dx.doi.org/10.1016/j. ophtha.2006.09.033.
- [11] S.S. Hayreh, Orbital vascular anatomy, Eye 20 (10) (2006) 1130–1144, http://dx.doi.org/10.1038/sj.eye.6702377, arXiv:0950-222X.
- [12] A. Harris, G. Guidoboni, B. Siesky, S. Mathew, A.C. Verticchio Vercellin, L. Rowe, J. Arciero, Ocular blood flow as a clinical observation: Value, limitations and data analysis, Prog Retin Eye Res. 24 (January) (2020) 100841, http://dx.doi.org/10.1016/j.preteyeres.2020.100841, URL: https://doi.org/10.1016/j.preteyeres.2020.100841.
- [13] Z. Burgansky-Eliash, H. Barash, D. Nelson, A. Grinvald, A. Sorkin, A. Loewenstein, A. Barak, Retinal blood flow velocity in patients with age-related macular degeneration, Current Eye Res. 39 (3) (2014) 304–311, http://dx.doi.org/10.3109/02713683.2013.840384.

- [14] T.A. Ciulla, A. Harris, H.S. Chung, R.P. Danis, L. Kagemann, L. McNulty, L.M. Pratt, B.J. Martin, Color doppler imaging discloses reduced ocular blood flow velocities in nonexudative age-related macular degeneration, Am. J. Ophthalmol. 128 (1) (1999) 75–80, http://dx.doi.org/10.1016/S0002-9394(99)00061-6.
- [15] B. Lee, J. Ahn, C. Yun, S.W. Kim, J. Oh, Variation of retinal and choroidal vasculatures in patients with age-related macular degeneration, Investigative Ophthalmology and Visual Science 59 (12) (2018) 5246–5255, http://dx.doi. org/10.1167/iovs.17-23600.
- [16] A. Harris, M. Harris, T.A. Ciulla, B. Martin, Aging affects the retrobulbar circulation differently in women and men, Arch Ophthalmol. 118 (2000) 1076–1080
- [17] T.A. Ciulla, A. Harris, L. Kagemann, R.P. Danis, L.M. Pratt, H.S. Chung, D. Weinberger, H.J. Garzozi, Choroidal perfusion perturbations in non-neovascular age related macular degeneration, Br J Ophthalmol. 86(2) (2002) 209–213.
- [18] E. Rechtman, A. Harris, B. Siesky, L. Kagemann, R.P. Danis, D. Sines, T.A. Ciulla, The relationship between retrobulbar and choroidal hemodynamics in nonneovascular age-related macular degeneration, Ophthalmic Surg Lasers Imaging 38 (3) (2007) 219–225. http://dx.doi.org/10.3928/15428877-20070501-06.
- [19] L. Chen, J.D. Messinger, K.R. Sloan, T.A. Swain, Y. Sugiura, L.A. Yannuzzi, C.A. Curcio, K.B. Freund, Nonexudative macular neovascularization supporting outer retina in age-related macular degeneration: A clinicopathologic correlation, Ophthalmology 127 (7) (2020) 931–947, http://dx.doi.org/10.1016/j.ophtha. 2020.01.040, URL: https://doi.org/10.1016/j.ophtha.2020.01.040.
- [20] P. Causin, G. Guidoboni, F. Malgaroli, R. Sacco, A. Harris, Blood flow mechanics and oxygen transport and delivery in the retinal microcirculation: multiscale mathematical modeling and numerical simulation, Biomech. Model. Mechanobiol. 15 (3) (2016) 525–542, http://dx.doi.org/10.1007/s10237-015-0708-7.
- [21] S.J. Cringle, Y. Dao-Yi, A multi-layer model of retinal oxygen supply and consumption helps explain the muted rise in inner retinal PO2 during systemic hyperoxia, Comp. Biochem. Physiol. A Mol. Integr. Physiol. 132 (1) (2002) 61–66.
- [22] M.W. Roos, Theoretical estimation of retinal oxygenation during retinal detachment, Comput. Biol. Med. 37 (6) (2004) 890–896, http://dx.doi.org/10.1016/j.compbiomed.2006.09.005, URL: http://dx.doi.org/10.1016/j.compbiomed.2006.09.005.
- [23] C. Brendan, J. Arciero, A. Harris, B. Siesky, Blood flow regulation and oxygen transport in a heterogeneous model of the mouse retina, Math. Biosci. 329 (2020) 108476
- [24] J. Arciero, A. Harris, B. Siesky, A. Amireskandari, V. Gershuny, A. Pickrell, G. Guidoboni, Theoretical analysis of vascular regulatory mechanisms contributing to retinal blood flow autoregulation, Invest. Ophthalmol. Vis. Sci. 54 (4) (2013) 5584–5593.
- [25] S. Cassani, A. Harris, B.A. Siesky, J. Arciero, Theoretical analysis of the relationship between changes in retinal blood flow and ocular perfusion pressure, J. Coupled Syst. Multiscale Dyn. 3 (1) (2015) 38—46.
- [26] L. Carichino, A. Harris, G. Guidoboni, B. Siesky, L. Pinto, E. Vandewalle, O. Olafsdottir, S. Hardarson, K. Van Keer, I. Stalmans, E. Stefansson, J. Arciero, A theoretical investigation of the increase in venous oxygen saturation levels in advanced glaucoma patients, J. Model. Ophthalmol. 1 (1) (2016) 64—87.
- [27] K.J. McHugh, D. Li, J.C. Wang, L. Kwark, J. Loo, V. Macha, S. Farsiu, L.A. Kim, M. Saint-Geniez, Computational modeling of retinal hypoxia and photoreceptor degeneration in patients with age-related macular degeneration, PLoS One 14 (6) (2019) e0216215.
- [28] L. Terry, N. Cassels, K. Lu, J.H. Acton, T.H. Margrain, R.V. North, J. Fergusson, N. White, A. Wood, Automated retinal layer segmentation using spectral domain optical coherence tomography: Evaluation of inter-session repeatability and agreement between devices, PLoS ONE 11 (9) (2016) 1–15, http://dx.doi.org/10.1371/journal.pone.0162001, arXiv:arXiv:1208.5792v1.
- [29] J.P. Campbell, M. Zhang, T.S. Hwang, S.T. Bailey, D.J. Wilson, Y. Jia, D. Huang, Detailed vascular anatomy of the human retina by projection-resolved optical coherence tomography angiography, Sci. Rep. 7 (February) (2017) 1–11, http://dx.doi.org/10.1038/srep42201.
- [30] R.A. Linsenmeier, Oxygen distribution and consumption in the cat retina during normoxia and hypoxemia, The J. General Physiol. 99 (2) (1992) 177–197, http:// dx.doi.org/10.1085/jgp.99.2.177, URL: http://jgp.rupress.org/content/99/2/177. abstract

- [31] B.W. Pogue, J.A. O'Hara, C.M. Wilmot, K.D. Paulsen, H.M. Swartz, Estimation of oxygen distribution in RIF-1 tumors by diffusion model-based interpretation of pimonidazole hypoxia and eppendorf measurements estimation of oxygen distribution in RIF-1 tumors by diffusion model-based interpretation of pimonidazole hypoxia, Radiat. Res. 155 (1) (2001) 15–25, http://dx.doi.org/10.1667/0033-7587(2001)155[0015:EOODIR]2.0.CO;2.
- [32] R.A. Ganfield, P. Nair, W.J. Whalen, Mass transfer, storage, and utilization of O2 in cat cerebral cortex, Am. J. Physiol. 219 (3) (1970) 814–&, http://dx.doi.org/10.1152/ajplegacy.1970.219.3.814.
- [33] D.Y. Yu, S.J. Cringle, Oxygen distribution and consumption within the retina in vascularised and avascular retinas and in animal models of retinal disease, Progr. Retinal Eye Res. 20 (2) (2001) 175–208, http://dx.doi.org/10.1016/S1350-9462(00)00027-6.
- [34] E. Rahimy, L. Kuehlewein, S.R. Sadda, D. Sarraf, Paracentral acute middle maculopathy, Retina, the J. Retin. Vitreous Dis. 35 (10) (2015) 1921–1930.
- [35] J.C. Arciero, B.E. Carlson, T.W. Secomb, Theoretical model of metabolic blood flow regulation: roles of ATP release by red blood cells and conducted responses, AJP: Heart Circ. Physiol. 295 (4) (2008) H1562–H1571, http://dx.doi.org/ 10.1152/ajpheart.00261.2008, URL: http://ajpheart.physiology.org/cgi/doi/10. 1152/ajpheart.00261.2008.
- [36] G. Chiaravalli, A virtual laboratory for retinal physiology: a theoretical study of retinal oxygenation in healthy and disease, (Ph.D. thesis), Politecnico di Milano, 2018, URL: https://www.politesi.polimi.it/handle/10589/145364.
- [37] G. Guidoboni, A. Harris, S. Cassani, J. Arciero, B. Siesky, A. Amireskandari, L. Tobe, P. Egan, I. Januleviciene, J. Park, Intraocular pressure, blood pressure, and retinal blood flow autoregulation: A mathematical model to clarify their relationship and clinical relevance, Invest. Ophthalmol. Visual Sci. 55 (7) (2014) 4105–4118, http://dx.doi.org/10.1167/iovs.13-13611.
- [38] J.D. Reynolds, S. Olitsky, Pediatric Retina, Springer-Verlag Berlin Heidelberg, 2011, http://dx.doi.org/10.1007/978-3-642-12041-1.
- [39] J. Deepa, T. Kuriakose, S. Devasahayam, A. Braganza, Dimensions of the foveal avascular zone using the Heidelberg retinal angiogram-2 in normal eyes, Indian J. Ophthalmol. 59 (1) (2011) 9–11, http://dx.doi.org/10.4103/0301-4738.73706.
- [40] A. Quarteroni, A. Valli, Numerical Approximation of Partial Differential Equations, Springer Series in Computational Mathematics, 23, Springer-Verlag Berlin Heidelberg, 1994.
- [41] F. Hecht, New development in freefem++, J. Numer. Math. (2012).
- [42] K. Pappelis, L. Choritz, N.M. Jansonius, Microcirculatory model predicts blood flow and autoregulation range in the human retina: in vivo investigation with laser speckle flowgraphy, Am. J. Physiol. (2020) H1253–H1273, http://dx.doi. org/10.1152/ajpheart.00404.2020.
- [43] R.A. Linsenmeier, H.F. Zhang, Retinal oxygen: from animals to humans, Progr. Retinal Eye Res. 58 (2017) 115–151, http://dx.doi.org/10.1016/j.preteyeres. 2017.01.003.
- [44] K.K.W. Chan, F. Tang, C.C.Y. Tham, A.L. Young, C.Y. Cheung, Retinal vasculature in glaucoma: a review, BMJ Open Ophthalmol. 1 (1) (2017) http://dx.doi.org/ 10.1136/bmjophth-2016-000032.
- [45] J. Arciero, L. Carichino, S. Cassani, G. Guidoboni, Mathematical modeling of blood flow in the eye, in: G. Guidoboni, A. Harris, R. Sacco (Eds.), Ocular Fluid Dynamics. Anatomy, Physiology, Imaging Techniques, and Mathematical Modeling, Springer-Birkhauser, New York, 2019, pp. 101–157.
- [46] D. Prada, A. Harris, G. Guidoboni, B. Siesky, A.M. Huang, J. Arciero, Autoregulation and neurovascular coupling in the optic nerve head, Surv. Ophthalmol. 61 (2) (2016) 164–186, http://dx.doi.org/10.1016/j.survophthal.2015.10.004, URL: https://www.sciencedirect.com/science/article/pii/S0039625715001824.
- [47] A. Harris, G. Guidoboni, B. Siesky, S. Mathew, A.C. Verticchio Vercellin, L. Rowe, J. Arciero, Ocular blood flow as a clinical observation: Value, limitations and data analysis, Progr. Retinal Eye Res. 78 (2020) 100841, http://dx.doi.org/10.1016/j.preteyeres.2020.100841, URL: https://www.sciencedirect.com/science/article/pii/S1350946220300136.
- [48] D.S.W. Ting, L.R. Pasquale, L. Peng, J.P. Campbell, A.Y. Lee, R. Raman, G.S.W. Tan, L. Schmetterer, P.A. Keane, T.Y. Wong, Artificial intelligence and deep learning in ophthalmology, British J. Ophthalmol. 103 (2) (2019) 167–175, http://dx.doi.org/10.1136/bjophthalmol-2018-313173.
- [49] G. Guidoboni, R.S. Chong, N. Marazzi, M. Chee, J. Wellington, E. Lichtenegger, C. Cheng, A. Harris, A mechanism-driven algorithm for artificial intelligence in ophthalmology: understanding glaucoma risk factors in the Singapore Eye Diseases Study, in: Annual Meeting of Association for Research in Vision and Ophthalmology (ARVO) Baltimore, MD, USA, 2020.